Ocean Sci., 9, 1057–1069, 2013
www.ocean-sci.net/9/1057/2013/
doi:10.5194/os-9-1057-2013

Ocean Science Open Access

Atlantic meridional ocean heat transport at 26° N: impact on subtropical ocean heat content variability

M. Sonnewald[1,2], J. J.-M. Hirschi[1], R. Marsh[3], E. L. McDonagh[1], and B. A. King[1]

[1]National Oceanography Centre, Southampton, Southampton SO14 3ZH, UK
[2]Institute for Complex Systems Simulation, University of Southampton, Southampton, SO17 1BJ, UK
[3]School of Ocean and Earth Science, National Oceanography Centre, University of Southampton, Southampton SO14 3ZH, UK

Correspondence to: M. Sonnewald (m.sonnewald@noc.soton.ac.uk)

Received: 30 November 2012 – Published in Ocean Sci. Discuss.: 10 January 2013
Revised: 30 September 2013 – Accepted: 21 October 2013 – Published: 5 December 2013

Abstract. Local climate is significantly affected by changes in the oceanic heat content on a range of timescales. This variability is driven by heat fluxes from both the atmosphere and the ocean. In the Atlantic the meridional overturning circulation is the main contributor to the oceanic meridional heat transport for latitudes south of about 50° N. The RAPID project has been successfully monitoring the Atlantic meridional overturning at 26° N since 2004. This study demonstrates how these data can be used to estimate the variability of the basin-wide ocean heat content in the upper 800 m between 26 and 36° N. Traditionally the atmosphere is seen to dominate the ocean heat content variability. However, previous studies have looked at smaller areas in the Gulf Stream region, finding that the ocean dominates deseasoned fluctuations of ocean heat content, while studies of the whole North Atlantic region suggest that the atmosphere may be dominant. In our study we use a box model to investigate fluctuations of the ocean heat content in the subtropical North Atlantic between 26° and 36° N. The box model approach is validated using 19 yr of high-resolution general circulation model (GCM) data. We find that in both the GCM- and RAPID-based data the ocean heat transport dominates the deseasoned heat content variability, while the atmosphere's impact on the ocean heat content evolution stabilizes after 6 months. We demonstrate that the utility of the RAPID data goes beyond monitoring the overturning circulation at 26° N, and that it can be used to better understand the causes of ocean heat content variability in the North Atlantic. We illustrate this for a recent decrease in ocean heat content which was observed in the North Atlantic in 2009 and 2010. Our results suggest that most of this ocean heat content reduction can be explained by a reduction of the meridional ocean heat transport during this period.

1 Introduction

The meridional heat transport (MHT) in the North Atlantic is a key climate variable, and is particularly important for northwestern Europe. We observe large regional changes in ocean heat content (OHC) due to MHT variability (Domingues et al., 2008). Moreover, as well as spatial MHT fluctuations, the MHT also varies on timescales from months to centuries and longer. Due to the MHT's importance in the climate system, much effort has gone into understanding and observing its variability and that of the meridional overturning circulation (MOC) (e.g. Bryden et al., 2005; Cunningham et al., 2007). Motivated by this, the RAPID mooring array has been delivering continuous observations of the Atlantic MOC at 26° N since 2004 (Johns et al., 2011; Rayner et al., 2011; McCarthy et al., 2012), and in this paper we demonstrate its utility towards estimating OHC variability through its close association with the MHT.

The ocean plays a major role in the northward transport of heat, and is particularly interesting because of its capacity to store heat. Together, the atmosphere and ocean act to redistribute the solar heating away from the Equator (Kump et al., 1999; Bryden and Imawaki, 2001; Jayne and Marotzke, 2001). Locally, the rate of heat content change in a body of water is determined as the balance of the energy flux through

its boundaries. Thus, if the boundary fluxes are known, the heat content can be determined.

The partitioning of the transport between the ocean and atmosphere has been widely discussed in the literature by, for example, Bryden and Imawaki (2001), and more recently by Fasullo and Trenberth (2008). They highlight that the partitioning of the heat transport and its effect on OHC is complex and varies with latitude. In the Northern Hemisphere, estimates by Trenberth and Caron (2001) suggest that the ocean dominates the MHT between 0° and 17° N, and towards higher latitudes the dry atmospheric transport carries an increasing fraction of the heat. However, the latent heat transport also transports an increasing fraction, and can be interpreted as a joint effort of the ocean and atmosphere. The area around 30° N is a very interesting region, as the ocean, atmosphere and latent heat transports contribute approximately equally to the overall MHT, and maximal poleward heat transport occurs at 35° N (Bryden and Imawaki, 2001; Trenberth and Caron, 2001; Fasullo and Trenberth, 2008). In this study, we focus on a basin-wide North Atlantic region between 26° and 36° N to capture these effects.

The complex partitioning between the atmosphere and ocean makes it difficult to determine the mechanisms behind OHC variability. Bjerknes (1964) examined North Atlantic sea surface temperature (SST) and sea level pressure (SLP) fields, leading him to the conclusion that the deseasoned SST variability was forced by the air–sea interactions. Gill and Niiler (1973) provided further evidence that the advection and mixing terms were small in the large-scale surface ocean heat budget, implying that the circulation in the North Atlantic is less important than local changes in heat storage and surface heat fluxes. Similarly, using monthly surface marine forcing, Cayan (1992) concluded that the large-scale atmospheric circulation controls the SST through changes in the air–sea heat flux. Seager et al. (2000) reached the same conclusion using model and reanalysis data, but suggest that the atmosphere operates on timescales which are too short to account for the low-frequency variability fully. In contrast, studies using general circulation models (GCMs) by Grötzner et al. (1998) as well as by Deser and Blackmon (1993) and Kushnir (1994) using surface observations suggest that the decadal mode is inherently a coupling between the ocean and the atmosphere expressed through unstable air–sea interactions. More recently, Dong and Sutton (2005) suggest that the Atlantic thermohaline circulation is forced by the atmosphere, but that the timescale is set by the ocean. A modelling study by Grist et al. (2010) complements this, finding that the surface heat flux only plays a small role in the deseasoned OHC variability away from the tropics.

Dong et al. (2007) investigate the relation between the surface flux and OHC in a region of the western boundary within the subtropical North Atlantic between 1992 and 1999. Using temperature profiles from the Global Temperature Salinity Profile Program (GTSPP) and an inverse modelling technique, they show that deseasoned changes in OHC cannot be explained by looking only at the surface flux. This is consistent with the complementary studies by Dong and Kelly (2004) and Vivier et al. (2002) with similar conclusions, dealing with the Gulf Stream and Kuroshio regions, respectively. Dong and Kelly (2004) present a thermodynamic model of the western boundary current region, between 30–45° N and 40–75° W, looking at the surface 400 m from 1992 to 1999, forcing their model with observed temperatures, estimates of geostrophic velocities from altimeter data and using NCEP/NCAR reanalysis data for surface heat flux and wind stress estimates. They conclude that the surface flux dominates the seasonal to deseasoned variability, but that the deseasoned upper-ocean heat content variability is dominated by advection–diffusion terms. Overall, our ability to assess the North Atlantic is improving through increasingly available observational data from the ocean and atmosphere, as well as improvements in ocean and atmosphere general circulation models. This work suggests that the North Atlantic OHC variability is dominated by the ocean on decadal timescales, while surface fluxes become increasingly important on shorter timescales.

A comparison of studies of OHC variability is difficult due to dependence on the location and timescales considered. Using observational data from the Argo float project, Hadfield et al. (2007) and Hadfield (2007) demonstrate that a heat budget analysis is possible, particularly in the subtropical North Atlantic. However, Hadfield (2007) suggests that the sampling resolution in space and time achieved by the floats may still underestimate heating from divergence. Studies by Dong and Kelly (2004) and Dong et al. (2007) rely on satellite altimetry to estimate geostrophic velocity, which is a valid approach in regions where large gradients in the sea surface height (SSH) occur, and avoids the problems highlighted by Hadfield et al. (2007) and Hadfield (2007). However, Hirschi et al. (2009) and Kanzow et al. (2009) demonstrate that accurate transport estimates cannot be obtained for basin-wide sections due to the decreased correlation between the SSH and the meridional transport close to continental margins.

In the present study we investigate the OHC variability in a basin-wide (i.e. margin to margin) region in the subtropical North Atlantic between 26° and 36° N. Particular emphasis is placed on illustrating the potential of the RAPID data at 26° N for understanding the causes of OHC variability. The paper is structured as follows: our methodology and the data used are presented in Sect. 2; a validation of the methodology and the results are presented in Sect. 3; and these are discussed and the paper concluded in Sect. 4.

2 Data and methods

A box model approach is used to study the OHC variability in the upper 800 m of a basin-wide section of the subtropical North Atlantic (26–36° N). We use two formulations of our box model. In the first advective formulation (hereafter

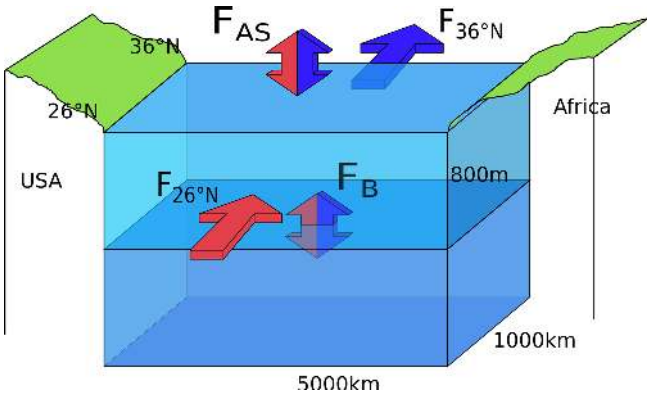

Fig. 1. Sketch illustrating the box model. Red and blue arrows indicate heat flux into and out of the box at 26° and 36° N, with the sign convention positive into the box. The blue/red arrows represent the air–sea surface flux and the mixing at the interface. There are no fluxes through the eastern and western sides.

referred to as the "AV box model"; see Sect. 2.2), we consider the advection of heat by the volume transport in the upper 800 m. In the second flux formulation (hereafter referred to as the "FV box model"; see Sect. 2.3), the OHC variability is estimated using the full depth MHT. The following sections describe the OCCAM data and RAPID-based observations used to force the box models, as well as the AV and FV formulations of the box model.

2.1 GCM and observational data

We use a 19 yr time series from the eddy-resolving 1/12° OCCAM, a primitive equation, level-coordinate, global oceanic general circulation model (OGCM). OCCAM has high vertical resolution, with 66 levels, 14 of which are in the top 100 m. The surface forcing for OCCAM consists of 6-hourly fields based on a blend of National Center for Atmospheric Research (NCAR) reanalysis and satellite data (Coward and de Cuevas, 2005; Marsh et al., 2009). The data from OCCAM are available from January 1988 to December 2006 with a temporal resolution of 5 days.

The RAPID-based observational ocean MHT data used in this study are from the RAPID–MOCHA project. Since April 2004, the RAPID–MOCHA observing system has been monitoring the Atlantic MOC at 26° N. The MOC is obtained by combining observations of the Florida Straits and Ekman transports, with a density-driven recirculation (Hirschi et al., 2003; Cunningham et al., 2007; Kanzow et al., 2007; Johns et al., 2011; McCarthy et al., 2012). Data from the RAPID–MOCHA observing system are available from 3 April 2004 to 1 January 2011 with a temporal resolution of 12 h. However, 5-day averages are used for consistency with the OCCAM data throughout our calculations.

The RAPID array was designed to monitor the MOC, but it can also be used to estimate the MHT. Johns et al. (2011) describe how the MHT is derived combining temperature transports from the Gulf Stream in the Florida Straits, the Ekman layer, the western boundary region offshore of the Bahamas and the interior ocean. This work revealed a correlation of 0.94 between the MOC and MHT, yielding the following relation (in PW, where $1\text{PW} = 10^{15}\text{W}$):

$$\text{MHT (PW)} = 0.079\text{MOC} + 0.12\text{PW}. \quad (1)$$

A strong relationship between MOC and MHT is also found in OCCAM where the correlation is 0.994.

For the period covered by the RAPID observations, we will also make use of observation-based OHC estimates calculated directly from Argo float data and from EN3 (Ingleby et al., 2007). EN3 was produced in the framework of the EU projects ENSEMBLES and ENACT and combine Argo data with other hydrographic data available during that period.

2.2 Advective version (AV) of the box model

Figure 1 illustrates the box model used to represent the top 800 m of the subtropical North Atlantic between 26° and 36° N. The oceanic heat content (OHC) is calculated using an Euler forward scheme with a 5-day time step:

$$\text{OHC}_{t+1} = \text{OHC}_t + \frac{\partial \text{OHC}}{\partial t}\Delta t, \quad (2)$$

$$\frac{\partial \text{OHC}}{\partial t} = F_{26^\circ\text{N}}(t) + F_{36^\circ\text{N}}(t) + F_{\text{AS}}(t) + F_{\text{B}}(t). \quad (3)$$

Here $F_{26^\circ\text{N}}$ and $F_{36^\circ\text{N}}$ are time series (defined in Eqs. 4 and 5 below) of MHT, F_{AS} the air–sea flux through the surface layer and F_{B} the exchange through the bottom interface. From OCCAM we use time series of MHT from the upper 800 m from 26° and 36° N available as 5-day averages. The MHT time series for $F_{26^\circ\text{N}}$ and $F_{36^\circ\text{N}}$ are calculated as

$$F_{26^\circ\text{N}}(t) = \int_{x_\text{E}}^{x_\text{W}} \int_{0}^{800} v_{26^\circ\text{N}}(x,z,t) T_{26^\circ\text{N}}(x,z,t) \rho c_\text{p} \text{d}z\text{d}x, \quad (4)$$

$$F_{36^\circ\text{N}}(t) = \int_{x_\text{E}}^{x_\text{W}} \int_{0}^{800} v_{36^\circ\text{N}}(x,z,t) T_{36^\circ\text{N}}(x,z,t) \rho c_\text{p} \text{d}z\text{d}x. \quad (5)$$

Here $v_{26^\circ\text{N}}$ and $v_{36^\circ\text{N}}$ are the velocity components normal to the sections through longitude-depth sections at 26° N and 36° N down to a depth of 800 m. $T_{26^\circ\text{N}}$ and $T_{36^\circ\text{N}}$ are the temperatures at the southern (26° N) and northern (36° N) interfaces of the box. The average density is denoted by ρ ($\rho = 1025\,\text{kg}\,\text{m}^{-3}$), and c_p is the specific heat capacity ($c_\text{p} = 3850\,\text{J}\,\text{kg}^{-1}\,\text{K}^{-1}$). The variables $v_{26^\circ\text{N}}$, $v_{36^\circ\text{N}}$, $T_{26^\circ\text{N}}$ and $T_{36^\circ\text{N}}$ were retrieved from the OCCAM model. $F_{26^\circ\text{N}}$ and $F_{36^\circ\text{N}}$ include contributions from the wind-driven, eddy

and gyre circulation, but ignore horizontal mixing, which we assume to be small. The terms $F_{26^\circ\mathrm{N}}$, $F_{36^\circ\mathrm{N}}$ and F_{AS} for the AV box model are illustrated in the left panel of Fig. 2.

To calculate the exchange through the bottom interface (F_{B}, used in Eq. 3), we use the relationship between the volume components ($V_{26^\circ\mathrm{N}}$ and $V_{36^\circ\mathrm{N}}$) entering and leaving the sides of the section, and thus determine the direction and magnitude of the heat flux to the lower layer F_B according to

$$F_{\mathrm{B}}(t) = -(V_{26^\circ\mathrm{N}}(t) - V_{36^\circ\mathrm{N}}(t))T_{\mathrm{interface}}(t)\rho c_{\mathrm{p}}, \quad (6)$$

where $T_{\mathrm{interface}}$ is the average temperature at the 800 m interface retrieved from the OCCAM model. Thus, for a net inflow of water into the box, there is a flux of heat to the deep and vice versa. The air–sea flux field was retrieved from OCCAM for the area of F_{AS}.

We focus on the variability and do not discuss trends in either the model or RAPID-based data. Thus, the work presented is based on detrended fluxes where the linear trend is removed, but we retain the temporal mean. Furthermore, for the first time step, the OHC is calculated with a set of initial values retrieved from the OCCAM model. For subsequent time steps, the temperature (T) of the ocean box is calculated using the volume of the ocean box (V, kept fixed at $5.4 \times 10^{15}\mathrm{m}^3$ as in the OCCAM model), the average density ($\rho = 1025\,\mathrm{kg\,m^{-3}}$) and the specific heat capacity ($c_{\mathrm{p}} = 3850\,\mathrm{J\,kg^{-1}\,K^{-1}}$):

$$T(t) = \frac{\mathrm{OHC}(t)}{V\rho c_{\mathrm{p}}}. \quad (7)$$

2.3 Flux version (FV) of the box model

For the FV box model, we use the RAPID-based data from 26° N. As only the full depth-integrated transport is available from RAPID, the FV of the box model reflects this by assuming that any net transport acts to increase the OHC in the surface box. Thus, we assume $F_{\mathrm{B}} = 0$ as opposed to depth exchanges being possible through an F_{B} term. The oceanic heat content (OHC) is again calculated using an Euler forward scheme with a 5-day time step:

$$\frac{\partial \mathrm{OHC}}{\partial t} = F^*_{26^\circ\mathrm{N}}(t) + F^*_{36^\circ\mathrm{N}}(t) + F_{\mathrm{AS}}(t). \quad (8)$$

The air–sea flux (F_{AS}) is identical to that used in AV up to 2006, and a seasonally varying climatology is used thereafter. The ocean heat fluxes $F^*_{26^\circ\mathrm{N}}$ and $F^*_{36^\circ\mathrm{N}}$ are the net heat fluxes over the entire section from the surface to the sea floor. The RAPID-based MOC data at 26° N are used to calculate $F^*_{26^\circ\mathrm{N}}$ as the MHT at 26° N according to Eq. 1.

No observational MHT time series exists at 36° N covering the period 2004 to 2011. However, as Grist et al. (2009) and Josey et al. (2009) demonstrate, there is a strong meridional coherence of the MOC in the study area. This was exploited, and $F^*_{36^\circ\mathrm{N}}$ is obtained using the relationship between the transport at 26° and 36° N in the OCCAM model, together with the lag in the OCCAM data between the two latitudes of 2.5 months (MHT at 26° N leads MHT at 36° N). A strong linear relationship is not immediately evident between the MHT at 26° and 36° N in the OCCAM model (Fig. 3, blue curve). Thus, to determine a more robust relationship between 26° and 36° N, we use a low-frequency filter (cut-off $3.7\,\mathrm{cycles\,yr^{-1}}$) and obtain an increased correlation (Fig. 3, red curve). We obtain the following linear regression:

$$F^*_{36^\circ\mathrm{N}}(t) = 1.57 \times 10^{-3}\mathrm{PW} + 0.682 \times F^*_{26^\circ\mathrm{N}}(t - \mathrm{lag}), \quad (9)$$

where 1.57×10^{-3} PW and 0.682 are constants obtained by fitting the linear model and the lag is 2.5 months. The terms $F^*_{26^\circ\mathrm{N}}$, $F^*_{36^\circ\mathrm{N}}$ and F_{AS} for the FV box model are illustrated in the right panel of Fig. 2.

2.4 Deseasoned and seasonally varying climatological MHT

We used the AV and FV box models together with their respective RAPID-based and OCCAM model-derived forcing to determine the OHC variability in the 800 m surface box. To investigate the seasonal component of the heat transport, the seasonally varying climatological year was constructed using the arithmetic mean of matching 5-day segments as in Atkinson et al. (2010). This gives an estimate of the purely seasonal variability. Removing this from the full forcing, we obtain an estimate of the deseasoned component which consists of the interannual variability and of the non-seasonal subannual variability:

$$\mathrm{MHT}_{\mathrm{deseasoned}} = \mathrm{MHT} - \mathrm{MHT}_{\mathrm{Clim}}. \quad (10)$$

2.5 Error estimates

We used the OCCAM model to validate our AV and FV box models, by retrieving the OHC for the equivalent box in the OCCAM model. To assess the errors resulting from the assumptions underlying the AV and FV box models, we compare the box model results to the full and deseasoned OCCAM model OHC variability. For a fair assessment of the FV box model, we use the full depth MHT from 26° N, retrieved from the OCCAM model, for the $F^*_{26^\circ\mathrm{N}}$ term, and infer $F^*_{36^\circ\mathrm{N}}$. Thus we can assess the impact of the missing F_{B} term, and of the assumptions made for $F^*_{36^\circ\mathrm{N}}$. We assess the error using the standard deviation (StD) of the difference from the OCCAM model OHC time series. For example for the AV OHC time series,

$$\mathrm{error} = \mathrm{StD}(\mathrm{OCCAM} - \mathrm{AV}). \quad (11)$$

Since we are interested in the OHC variability, the time mean is removed from the OHC time series. As a consequence taking the StD is equivalent to the root mean square error (RMSE).

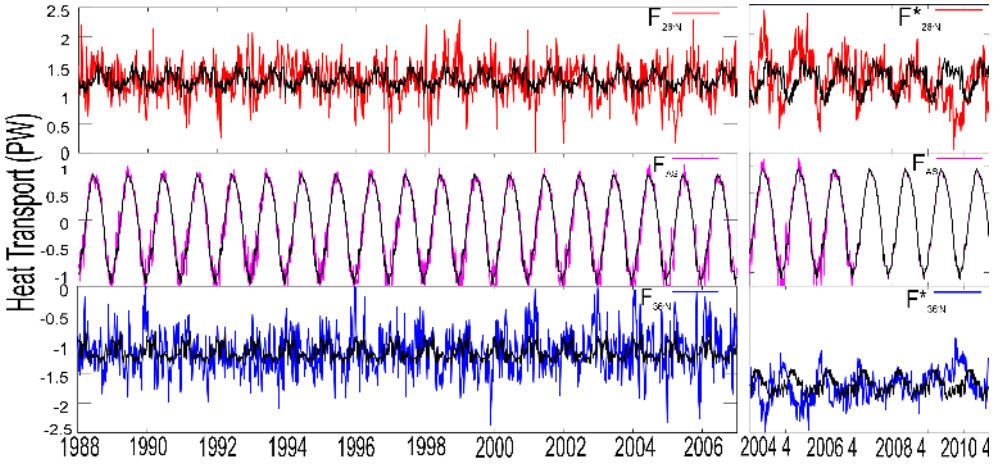

Fig. 2. The MHT and air–sea flux (PW) used to force the box model, for AV (left, as described in Sect. 2.2) and FV (right, as described in Sect. 2.3, starting in April 2004) experiments. Positive (red) transports enter the box at 26° N, while negative transports (blue) leave the box at 36° N. The air–sea flux (F_{AS}, magenta) can be positive or negative. Black lines illustrate the seasonally varying climatology components of the respective forcing. For the F_{AS} component for the observational case, the OCCAM-derived NCAR forcing was used up to December 2006, and the seasonally varying climatology thereafter. The right figure starts in April 2004, as this is when the RAPID-based estimates become available.

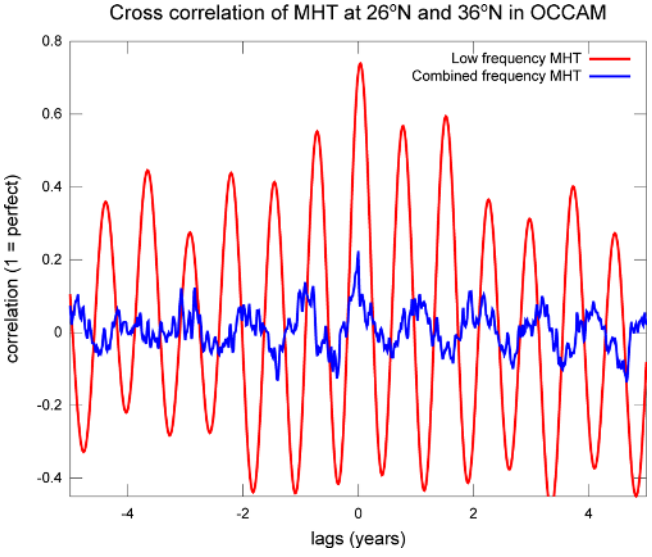

Fig. 3. Figure illustrating the change in cross-correlation investigating the full (combined, blue) and the low-frequency (red) heat flux F_{26° and $F_{36^\circ\,N}$. To separate the high- and low-frequency transport, a low-pass filter was used. Here the cut-off frequency of 3.7 cycles/year was used, as a marked decrease in the variance of both $F_{26^\circ\,N}$ and $F_{36^\circ\,N}$ was observed using this.

Moreover, to assess the impact of inferring $F^*_{36^\circ\,N}$ from $F^*_{26^\circ\,N}$, we again use the FV box model formulation forced with full depth data from the OCCAM model. We compare the performance of our inferred $F^*_{36^\circ\,N}$ to the full OCCAM model. We also test the cases where $F^*_{36^\circ\,N} = 0$, and where we use only the low-frequency component of $F^*_{26^\circ\,N}$ to infer $F^*_{36^\circ\,N}$. We calculate the error as above, with reference to the full OCCAM model.

3 Results

As a first step, we present the full fluxes used to force the model. We then validate the advective and flux versions of the box model (AV and FV, respectively). This is followed by a series of experiments where the box model is subjected to different forcing scenarios.

3.1 Box model forcing

Figure 2 illustrates the heat fluxes used to force the AV and FV box models. Table 1 shows the StD, minimum and maximum of the heat transport. In both the AV and the FV case, the F_{AS} air–sea flux dominates the statistics with an StD of 0.71 PW. The $F_{26^\circ\,N}$ and $F_{36^\circ\,N}$ AV forcing have StDs of 0.28 and 0.35 PW, respectively. The $F^*_{26^\circ\,N}$ FV forcing has a higher StD of 0.37 PW, relative to the AV box model. The inferred $F^*_{36^\circ\,N}$ FV forcing has a smaller StD of 0.25 PW, as expected from the low-frequency-based inference process.

Figure 2 illustrates the values reported in Table 1. Here we can see the large amplitude of F_{AS}, which is dominated by the seasonally varying climatology. The $F_{26^\circ\,N}$ and $F_{36^\circ\,N}$ AV forcing terms are smaller in amplitude, and are less dominated by the seasonally varying climatology. Maximum transport occurs between late July and November, while minimum transports occur between mid-February and mid-March. At 36° N, maximum transport

Table 1. Table of minimum, maximum (PW) and StD (PW) values of the heat transports used (detrended and with the mean removed) for the AV (OCCAM) and FV (RAPID-based) box models. Transports into the box (ocean) and downwards (air–sea) are positive.

Forcing	Min	Max	StD
F_{AS}	−1.76	1.05	0.71
$F_{26° N}$	−1.20	0.99	0.28
$F_{36° N}$	−1.17	1.15	0.35
$F^*_{26° N}$	−1.18	1.17	0.37
$F^*_{36° N}$	−0.80	0.80	0.25
F_{AS} clim.	−1.20	0.90	0.47
$F_{26° N}$ clim.	0.80	1.28	0.11
$F_{36° N}$ clim.	0.57	1.08	0.12
$F^*_{26° N}$ clim.	−0.42	0.36	0.21
$F^*_{36° N}$ clim.	−0.25	0.27	0.25

occurs from mid-August to October, and minimum transport occurs from March to April.

For the $F^*_{26° N}$ and $F^*_{36° N}$ FV forcing terms, the seasonally varying climatology has a larger amplitude, but the short duration and the highly variable nature of the RAPID-based forcing means that the seasonally varying climatology is not as good at capturing the true seasonal signal. The maximum heat transport is found in June–November, and the minimum is found in January–March, as also reported by Johns et al. (2011) and Atkinson et al. (2010). These maximum and minimum transports are similar both at 26° and 36° N, differing by 2.5 months, as expected from our use of the regression model.

In both the AV and FV forcing, the amplitude of the seasonally varying climatology at 36° N is smaller than at 26° N, as demonstrated in Table 1, suggesting that the seasonality becomes less pronounced further away from the Equator in agreement with studies such as Jayne and Marotzke (2001) and Fasullo and Trenberth (2008).

3.2 Validating the box model

To validate the AV and FV box model formulations, we compare our OHC estimates to the OCCAM model OHC for the equivalent 800 m deep subtropical North Atlantic Ocean box, illustrated in Figs. 4 and 5. For convenience, we convert the OHC into temperature according to Eq. (7), and in the remainder of the paper OHC anomalies will be quantified in terms of temperature anomalies.

The AV box model in Fig. 4 is exactly as described in Sect. 2.2. The FV box model is as described in Sect. 2.3, but with $F^*_{26° N}$ derived from the equivalent OCCAM data, and $F^*_{36° N}$ inferred from $F^*_{26° N}$. Thus, we assess the fit of the FV box model as well as the assumptions underlying the FV box model: using full-depth fluxes for $F^*_{26° N}$, inferring $F^*_{36° N}$ and the missing F_B term. However, in both the AV and FV box models, we do not include diffusion or an eddy correlation term as described in Huerta-Casas and Webb (2012).

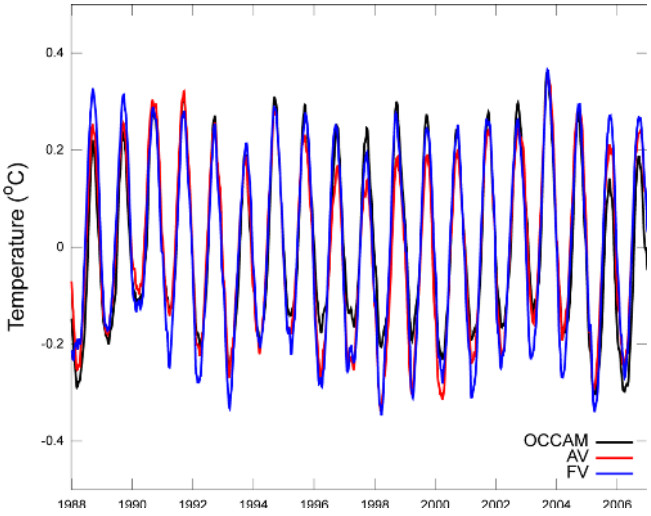

Fig. 4. Demonstration of box model performance, OHC detrended and with the mean removed. The black line is from the full OCCAM model, red line from the AV box model and the blue line from the FV box model run with data taken from OCCAM for $F^*_{26° N}$, using this to infer the $F^*_{36° N}$, but otherwise as described in Sect. 2.3. Both box model versions show good agreement with the OCCAM model, with StD of difference from the OCCAM model of 0.057 °C for the AV box model and 0.065 °C for the FV box model, compared to the StD of the full OCCAM model with an StD of 0.16 °C.

Figure 4 shows that the full AV and FV box models largely reproduce the OHC variability retrieved from the OCCAM model. We estimate the error according to Eq. (11). For the AV box model, the error is 0.057 °C, while the FV box model has an error of 0.065 °C. Both these errors are small compared to the StD of the full OCCAM model with an StD of 0.16 °C. Figure 4 illustrates that the amplitude of the seasonally varying climatology is well captured in both the AV and FV box models. The AV box model is overall closer to the full OCCAM model, but tends to exaggerate the winter cooling by approximately 0.01 °C. Overall, the FV box model also reproduces the OHC variability from the OCCAM model, but we observe deviations of up to 0.1 °C.

To illustrate the deviations of the AV and FV box models from the OCCAM model further, Fig. 5 shows the deseasoned component of the OHC variability. Here we remove the seasonally varying climatology from the forcing data, further illustrating that both the AV and the FV box models capture the OCCAM model variability well. Three major broad peaks (in the early and mid-1990s as well as between 2002 and 2005) lasting about 3 yr are visible in both the AV and FV box models and the OCCAM model, together with a sharp peak in early 1999. The AV box model has an error of 0.041 °C, while the StD of the deseasoned OCCAM model is 0.056 °C. The correlation between the AV box model and OCCAM is 0.72 (87 degrees of freedom, significant at the

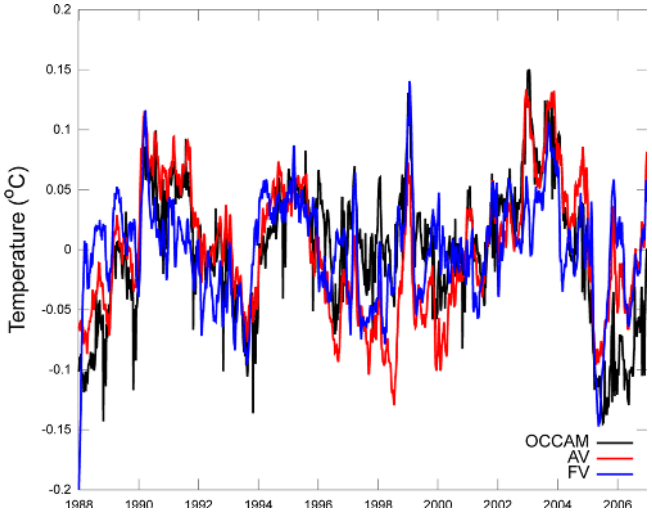

Fig. 5. Interannual detrended temperature variability in the OCCAM model (black) and box model AV (red), FV (blue), all detrended and with the mean removed. The AV box model is run as described in Sect. 2.2, while the FV box model is run with data taken from OCCAM for $F^*_{26^\circ\mathrm{N}}$, using this to infer the $F^*_{36^\circ\mathrm{N}}$, but otherwise as described in Sect. 2.3. We obtain the deseasoned components by removing the seasonally varying climatology. The AV box model deseasoned OHC StD of the deviation from the OCCAM model is 0.041 and 0.048 °C for the FV box model, while the StD of the deseasoned OCCAM model is 0.056 °C. This confirms that the box model can be used to investigate the full and deseasoned components of the oceanic and air–sea causes of OHC variability.

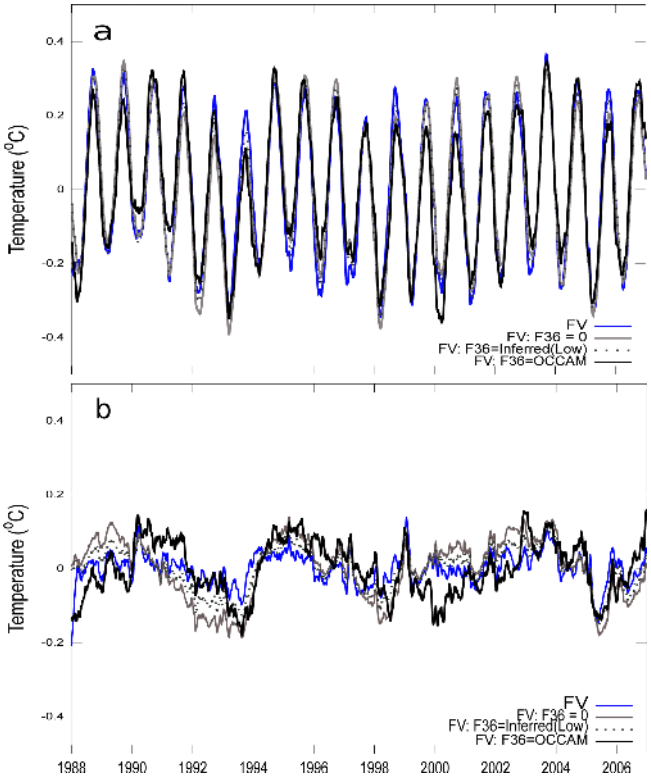

Fig. 6. Validating the assumptions for $F^*_{36^\circ\mathrm{N}}$ of the FV box model. Panel **(a)** shows the full signal, while panel **(b)** shows the deseasoned component. In both panels, the blue line is the FV box model as in Fig. 4. The black line shows the case where $F^*_{36^\circ\mathrm{N}}$ is derived from the OCCAM model. The grey line shows a case where $F^*_{36^\circ\mathrm{N}} = 0$. The dark grey stippled line shows the model using inferred forcing at 36° N obtained using only the low-frequency component of $F^*_{26^\circ\mathrm{N}}$. The high-frequency component was included in the FV box model using the RAPID-based data as $F^*_{26^\circ\mathrm{N}}$ to infer $F^*_{36^\circ\mathrm{N}}$.

99 % level). For the FV box model the agreement with OCCAM is less pronounced. The error is 0.048 °C and the correlation drops to 0.57 (110 degrees of freedom, significant at the 99 % level). The decrease in correlation can largely be explained by a decrease in the agreement between the FV box model and OCCAM for high (i.e. subannual) frequencies. When filtering the time series for OCCAM and the FV and AV box models (second-order Butterworth low-pass filter, cut-off at 0.9 cycles/year), the correlation is ≈ 0.7 for both the AV and the FV box model formulations (not shown). Figure 5 illustrates that the FV box model overestimates the increase in OHC from 1988 to the early 1990s, towards the mid- to late 1990s it tends to underestimate, and it overestimates from 2005 onwards. Overall, Fig. 5 confirms that both the AV and FV box models capture the OHC variability in the OCCAM model reasonably well. This agreement suggests that both the AV and FV box models can be used to gain insight into the oceanic and air–sea contributions of OHC variability.

Figure 6 illustrates the effect of the added assumptions from inferring the $F^*_{36^\circ\mathrm{N}}$ transport. This is demonstrated using the full depth data from the OCCAM model directly for $F^*_{26^\circ\mathrm{N}}$ and $F^*_{36^\circ\mathrm{N}}$. Figure 6a illustrates the full signal. We calculate the error as described in Sect. 2.5. Thus, by inferring $F^*_{36^\circ\mathrm{N}}$ from $F^*_{26^\circ\mathrm{N}}$ (equivalent to the situation we later have when using the full depth RAPID-based data), we have an error of 0.065 °C for the full signal, with a correlation with the OCCAM OHC of 0.94 (19 degrees of freedom), significant at the 99 % level. This is an improvement over the case where $F^*_{36^\circ\mathrm{N}} = 0$ with an error of 0.070 °C for the full signal, with a correlation with the OCCAM OHC of 0.92 (20 degrees of freedom), significant at the 99 % level. However, the regression model used to infer the $F^*_{36^\circ\mathrm{N}}$ transport was made using only the low-frequency transports from $F_{26^\circ\mathrm{N}}$ and $F_{36^\circ\mathrm{N}}$. For the FV box model forcing presented in Fig. 2, we infer $F^*_{36^\circ\mathrm{N}}$ using the full RAPID-based $F^*_{26^\circ\mathrm{N}}$ where both the high and low frequencies are present. If only the low frequency (cut-off 3.7 cycles yr^{-1}) is used, the error is still 0.067 °C for the full signal, with a correlation with the OCCAM OHC of 0.93 (19 degrees of freedom), significant at the 99 % level. However, we know that a high-frequency component should be present in $F^*_{36^\circ\mathrm{N}}$. Thus, our validation of the FV box model suggests that using the full $F^*_{26^\circ\mathrm{N}}$ to infer $F^*_{36^\circ\mathrm{N}}$ provides the

best available estimate of the OHC variability for the FV box model case.

Figure 6b illustrates the deseasoned component. This further highlights that inferring $F^*_{36^\circ\mathrm{N}}$ from $F^*_{26^\circ\mathrm{N}}$ provides the best estimate for $F^*_{36^\circ\mathrm{N}}$, when compared to retrieving $F^*_{36^\circ\mathrm{N}}$ from OCCAM. We also note that we find a similar correlation (0.57, 108 degrees of freedom, significant at the 99 % level) between the deseasoned time series from the FV box model with inferred $F^*_{36^\circ\mathrm{N}}$ and OCCAM. As before, the correlation increased to about 0.7 when a second-order Butterworth filter (cut-off at 0.9 cycles/year) was applied to the time series (independently of whether we retrieve $F^*_{36^\circ\mathrm{N}}$ from OCCAM or whether we infer this transport).

3.3 Partitioning OHC variability

Figure 7a illustrates the results of the AV box model forced with $F_{26^\circ\mathrm{N}}$ and $F_{36^\circ\mathrm{N}}$ derived from the OCCAM model. The seasonality in the MHT contributes very little to the overall seasonal OHC signal, and remains close to zero. The overall seasonally varying climatology of the OHC corresponds to a mean seasonal temperature range of $\approx 0.42\,^\circ$C, which is mainly due to the air–sea fluxes. The ocean therefore contributes little to the seasonal OHC variability. The deseasoned signal can be seen again to have three broad OHC maxima as well as the sharp 1999 peak. These broad maxima are seen to correspond to a broad peak in the spectral domain representing a signal with a period of 5–7 yr. Figure 7a reveals that this variability is accounted for by the deseasoned oceanic signal, which can be also seen to have three broad peaks. Overall, most of the variability in the deseasoned signal is accounted for by the oceanic MHT. The deseasoned atmospheric variability can be seen to affect the amplitude of the signal, but overall the oceanic heat transport dominates.

The same pattern is also found in the FV box model, forced with the RAPID-based MHT values for $F^*_{26^\circ\mathrm{N}}$ and inferring F?36?N (Figure 7b). The amplitude of the seasonally varying climatology of $\approx 0.45^\circ$C is dominated by the atmosphere, but is amplified slightly by the ocean, whose contribution is larger than in the AV box model. As before, the deseasoned signal is dominated by the ocean. The effect of the atmosphere can only be assessed to the end of 2006, since the air–sea fluxes from the OCCAM model are not available beyond 2006. However, the available timeline suggests that the deseasoned variability of the atmosphere has a smaller effect in the FV box model, changing the amplitude of the overall deseasoned signal only sightly. The deseasoned variability is higher before 2007, with two pronounced peaks that resemble a seasonal cycle. This disappears after 2007, and the signal stabilizes until mid-2009 where the signal drops from ≈ 0.1 to $-0.2\,^\circ$C. This dip is caused by the deseasoned oceanic signal since the atmospheric forcing does not contain any interannual variability from 2007 onwards.

Key OHC statistics is displayed in Fig. 8. These visualize the timescales over which the oceanic and atmospheric components of OHC tendency act, as well as their respective magnitude and variability. A sliding window technique is used to collect the maximum amplitude of temperature change within windows of a prescribed length. Sliding the window along the time series allows us to collect the median, first and third quartiles of peak-to-peak temperature variability. Shown are the median (solid coloured line) as well as the first and third quartiles (lower and upper bound of the coloured area, respectively) for the absolute magnitude ($|\Delta T|$) of OHC change for time windows ranging from 5 days up to 4 yr. Figure 8 demonstrates the gradual nature of the change in dominance on OHC variability between the seasonal atmospheric and deseasoned oceanic signals, as well as the likelihood of this occurring.

Figure 8a illustrates that in the AV box model, the seasonally varying climatological atmospheric component changes the OHC by 0.42 °C over 6 months. In contrast, the

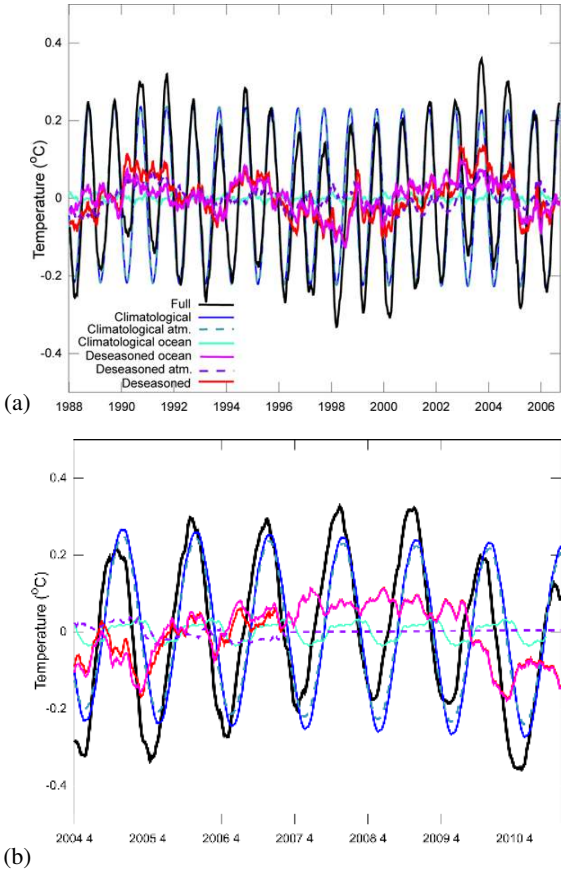

Fig. 7. Figure summarizing the AV **(a)** and FV **(b)** box model results, detrended and with the mean removed. Both figures illustrate the OHC variability attributable to the tested forcing scenarios. Note the atmospheric dominance on the seasonally varying climatology (referred to as "climatological") OHC variability, and the oceanic dominance of the deseasoned OHC variability. Panel **(b)** starts in April 2004, as this is when the RAPID-based estimates become available.

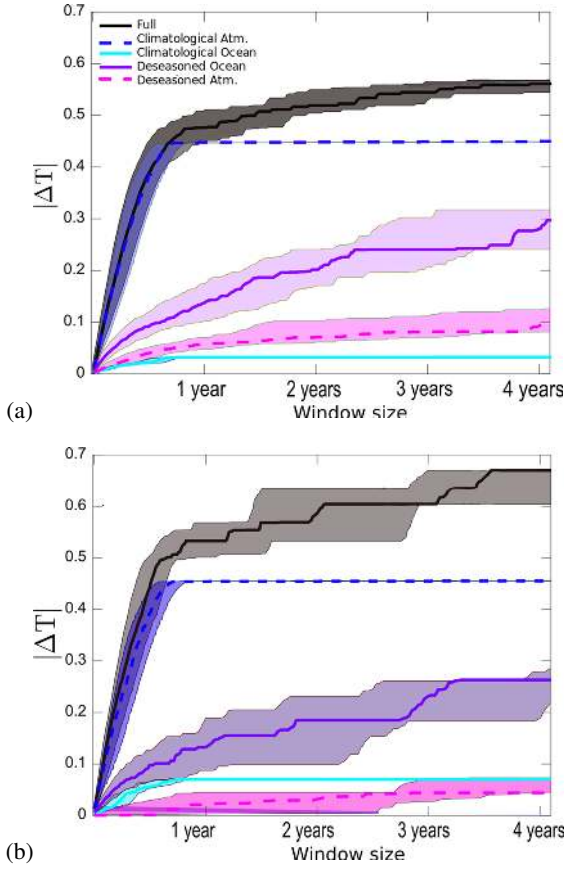

Fig. 8. The absolute magnitude of OHC change (|ΔT| in °C) attributed to each component. Coloured regions illustrate the respective first quartile (upper line), median (thick line) and third quartile (lower line) of the largest |ΔT| within a sliding window of an increasing size. The AV box model is indicated by **(a)**, while **(b)** shows the FV box model using the RAPID-based data. Note the OHC variability attributable to the seasonally varying climatology (referred to as "climatological") stabilizes within a year, while the importance of the deseasoned components increase with time/window size. Further, the figure highlights the partitioning between the components, illustrating the magnitude of the deseasoned component, and the timescales over which this has an impact.

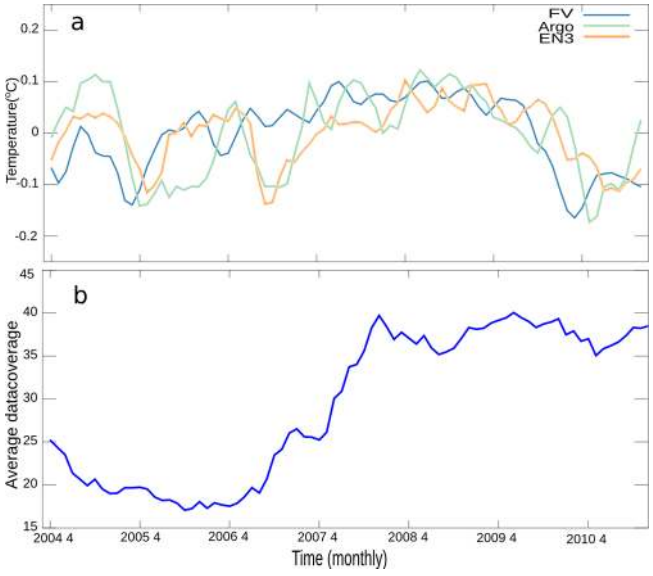

Fig. 9. (a) deseasoned OHC for the basin-wide North Atlantic section from 26° and 36° N. The FV (blue), Argo (green) and EN3 (yellow) data are shown. Note the good agreement after mid-2007, which is most likely due to the increased data coverage of the Argo floats. **(b)** the average number of Argo profiles in a 1500 km radius around each 2.5° grid point. The time of the RAPID-based time series is shown from April 2004 to January 2011.

seasonally varying climatological component of ocean heat transport only changes the temperature by 0.02 °C. However, over 4 yr the deseasoned oceanic component can contribute 0.3 °C, while the spread of the deseasoned atmospheric component contributes only 0.1 °C. The spread of the deseasoned oceanic component is at times more than 0.1 °C while the spread of the seasonally varying climatological atmosphere is around 0.05 °C. Further, the overall OHC variability follows the seasonal atmosphere closely up to 6 months. After this, the OHC change due to the deseasoned oceanic component steadily increases as the window length is increased. This confirms the dominance of the deseasoned oceanic variability on timescales exceeding 6 months, compared to the much smaller influence of deseasoned atmospheric variability.

Figure 8b shows a similar pattern for the FV box model. The overall OHC variability does not follow the seasonal atmosphere as closely, but a clear levelling after 6 months is observed. The same partitioning between the ocean and atmosphere is seen in the full and deseasoned OHC time series, but the seasonally varying climatological ocean has a larger influence than the deseasoned atmosphere. The spread of the deseasoned oceanic signal is also larger, which is reflected in the overall OHC variability. However, overall we see that in both the AV and the FV box models, the atmosphere contributes little to OHC variability on timescales beyond 6 months, while the oceanic influence contributes progressively at all considered timescales.

In a next step, we use the FV box model to interpret the recent OHC variability between 26° and 36° N as observed by Argo floats and in the EN3 data set (Ingleby et al., 2007). Figure 9a illustrates that the OHC evolution after mid-2007 is of particular interest. In EN3, Argo and the FV box model there is a period of reduced OHC variability from 2007 to 2008, followed by a pronounced decrease of OHC from 2009 to 2010. There are differences in the precise timing of the OHC reduction during this phase, but we see that in all three cases the temperature in the subtropical ocean box reduces by over 0.2 °C. The results from our FV box model strongly suggest that this decrease can largely be explained by a reduction in the MHT at 26° N, which coincided with the pronounced

MOC minimum described in McCarthy et al. (2012). Using our error estimates for the FV box model as demonstrated in Figs. 4 and 5, we note that this decrease is unlikely to be due to FV box model errors. We further note that the difference in timing of the 2009 to 2010 event is approximately 3 months, similar to the lag observed between 26° and 36° N in the OCCAM model. Thus, the earlier timing in our FV box model could be the result of using the average lag between 26° and 36° N, while the true ocean signal took longer to propagate to 36° N. An atmospheric "buffer" could also have been active in Argo and EN3: the atmosphere could have absorbed a fraction of the anomalous OHC, damping the OHC response. However, this would be less likely to have caused the observed OHC decrease if this were indeed associated with the MOC minimum as described in McCarthy et al. (2012). Furthermore, the lack of the F_B term could also contribute to the difference in timing through exchanges with the deep ocean. However, we note that the magnitude of our event is comparable to that in the Argo product, and thus unlikely to be due to the missing F_B.

Prior to 2007 we see a larger implied uncertainty in Fig. 9, where Argo and EN3 disagree with each other as much as with our FV box model. Differences between Argo and EN3 could be due to the observational data used in these products. The EN3 OHC uses uncalibrated Argo data as well as hydrographic observations, while only the delayed mode, quality controlled, Argo product is used for the Argo OHC product. Error estimates for Argo and EN3 are still in development due to uncertainties in the temporal and spatial correlation length scales (S. Good, personal communication, 2013). However, the discrepancy between Argo and EN3 could be due to the changes in data coverage. Between 2004 and 2011 the number of floats has increased, improving the accuracy of their OHC estimates. In Fig. 9b we show the average number of floats used in the estimation of the Argo product in Fig. 9a. The Argo product is estimated for $2.5° \times 2.5°$ grid cells, where the recorded temperature is a distance and data density weighted average for each box, where the radius used is 1500 km with a decorrelation length scale of 500 km. Figure 9b illustrates that a dramatic increase in the data coverage took place in 2007, with the Argo float fleet reaching its full global capacity of 3000 floats in November 2007. This coincides with the time where our FV box model, Argo and EN3 come to a reasonable agreement. However, the Argo floats are constrained largely to waters where the shelf is deeper than 2000 m, which could lead to errors in regions where large parts of the signal are on the shallower shelf, such as the transport through the Florida Straits.

4 Discussion and conclusion

In this study we demonstrate how RAPID-based data can be used to estimate the OHC variability in the subtropical North Atlantic using a box model budget analysis. For the area between 26 and 36° N, we construct advective and flux versions of the box model (AV and FV), respectively forced by the divergence of heat advection in the upper 800 m, and the divergence of the top-to-bottom meridional heat flux. We test the assumptions underpinning our box model approach using data from the high-resolution OCCAM model. Both versions of the box model simulate seasonal cycles of slightly higher amplitude than OCCAM (see Fig. 4). Larger seasonal signals in both the AV and FV box models indicate shortcomings in the box model simplifications (see further discussion below) and/or missing terms in the forcing. However, we find good correlations between the OCCAM model and our AV and FV box models. This confirms that our AV and FV box model approaches are valid for studying cases where linear trends are removed, but retaining the temporal mean. We evaluate the FV box model alongside OHC estimates based on Argo and EN3 data. Figure 9 illustrates that the OHC evolution is broadly similar in all three cases, especially after 2007, when the Argo fleet reached its full data coverage. After 2007 Argo, EN3 and our FV box model are in reasonable agreement, where a plateau through to 2009 is followed by a 0.2 °C dip in 2010 and a recovery thereafter. Our results strongly suggest that the reduction in OHC seen in 2009 and 2010 can largely be explained by a reduction in the MOC (and therefore MHT) during that period.

Caveats in the AV and FV box model include neglecting horizontal and vertical mixing. Furthermore, the 5-day averaging of output variables in the OCCAM model leads to inexact heat budget closure (Huerta-Casas and Webb, 2012). The averaging leads to underestimating the eddy correlation and any variable varying significantly within the 5-day window. However, the smaller OCCAM model seasonally varying climatology suggests a seasonality in the "missing" flux, which would be surprising in the presumably more chaotic sum of eddy correlations. A full investigation of this would require the instantaneous model fields and not just the 5-day averages. However, the differences between the AV and FV box models can possibly be attributed to the additional assumptions underlying the FV box model. The neglect of vertical heat exchange F_B increases the seasonal cycle, and the fit of the FV box model's deseasoned OHC does not follow the OCCAM model as closely. Furthermore, the F_B term assumes that any volume imbalance is immediately compensated by the deeper layer, using the average interface temperature. However, this process is not likely to be homogeneous across the bottom of our box. Thus, with volume imbalance from a flux of warmer (colder) water at the southern (northern) boundary, the F_B term is likely to be too small (large), due to our use of the average interface temperature. As we use detrended fluxes, differences in the trends in the forcing data could lead to deviations from the OCCAM model.

Josey (2001), Vivier et al. (2002), Dong and Kelly (2004) and Wells et al. (2009) suggest that using NCEP/NCAR forcing could overestimate the heat loss to the atmosphere through the latent and sensible heat flux terms. The OCCAM

model was forced using NCEP/NCAR surface forcing, and the F_{AS} used in both the AV and FV box model derived from the OCCAM model could be affected, meaning that our results could overestimate the atmospheric contribution. Using the OCCAM model-derived F_{AS} for both FV and AV allows us to keep the models as comparable as possible. Furthermore, a surface damping effect could also be introduced through the use of a reanalysis product to force the OCCAM model. The reanalysis data used to force the OCCAM model (Large et al., 1997; Marsh et al., 2009) use an atmospheric model guided by available data and surface ocean fields. Thus, due to the one-way communication across the ocean–atmosphere interface, feedbacks and possible amplifications will be damped. Spatial and temporal smoothing could also potentially lead to damping of the atmospheric signal. These caveats affect our AV and FV box models, as well as the OCCAM model. Furthermore, this could also be a source of error when comparing our FV box model data to the Argo and EN3 products.

Furthermore, the assumptions we make to infer $F^*_{36^\circ N}$ are a source of error in the AV box model. The chosen method minimizes the error, as estimated using the OCCAM OHC. However, since we do not have observational estimates at 36° N, the underlying assumptions of meridional coherence are key to the success of the inference, and we find that the different estimates assessed here have only a minor impact on the FV–OCCAM agreement. The wider applicability of our FV box model method using the RAPID-based data is likely constrained by the meridional coherence of the MOC. We chose a northern boundary of 36° N based on work by Bingham et al. (2007) and Grist et al. (2009), who illustrate that the character change of the circulation around 40° N would prevent use, further north, of the regression model to infer transport anomalies from those at 26° N. It would be necessary to base the regression model on lower frequency variability, in accordance with the reduced meridional coherence north of 40° N. However, results from Bingham et al. (2007) and Grist et al. (2009) indicate there could be potential for extending the model southwards to 10° N.

Despite the sources of errors discussed above, the models (OCCAM model, AV, FV) can reflect documented events. The FV box model shows a pronounced temperature dip in 2010. McCarthy et al. (2012) show that a significant fraction of the pronounced MOC reduction in 2009/2010 is due to a change in geostrophic transports, with associated cooling north of 25° N. The high correlation between MOC and MHT means that the geostrophic part of the MHT is likely to be a major contributor to the OHC reduction in 2009/2010. Our FV box model could underestimate the effect of a lag between 26 and 36° N, or a possible atmospheric "buffering", causing the 2009/2010 event to happen approximately 3 months before it is seen in the Argo data.

Overall, our results are in good agreement with previous similar studies such as Dong and Kelly (2004),Dong et al. (2007), Grist et al. (2010) and Wells et al. (2009). Our study also suggests that the results found in the more regional studies of Dong and Kelly (2004) and Dong et al. (2007) hold for a basin-wide section, and an extended time series. Investigating the Atlantic Ocean, Grist et al. (2010) found that the deseasoned signal in OHC variability is largely ocean-dominated in the subtropics and subpolar regions. Like Grist et al. (2010) we find similar results using modelled and observational OHC in the subtropical North Atlantic. However, this study used data from the eddy-resolving 1/12° GCM, whereas Grist et al. (2010) used an eddy-permitting 1/4° GCM. Further, we affirm the conclusions using observational Argo and EN3 data.

In conclusion, this study has examined the roles of the ocean and atmosphere in causing seasonal and deseasoned OHC variability in the subtropical North Atlantic. Here the effect of the non-seasonal ocean is of particular interest. This is because its large deseasoned variability makes it less predictable than the seasonal air–sea flux. We have demonstrated the utility of the RAPID-based data in studies of the OHC variability of the subtropical North Atlantic, confirming that the ocean dominates on deseasoned timescales gaining importance on longer timescales, while the influence of the atmospheric variability (on longer timescales) makes very little contribution to OHC variability at timescales less than 6 months. We can confirm the results of studies such as Dong and Kelly (2004) for a basin-wide section using both our FV and AV box models, but the success of the AV box model is tied to the strength of the meridional coherence of the MOC, and thus our method is limited to the latitudinal bounds south of 40° N as indicated by Bingham et al. (2007) and Grist et al. (2009). Our study supports ongoing work with studies including the RAPID-based data to enhance the interpretation of OHC from Argo observations. The utility of the RAPID-based data suggests that its inclusion can further our understanding of the underlying mechanisms driving OHC variability.

Acknowledgements. We acknowledge Andrew Coward as the primary developer of the 1/12° version of OCCAM, for undertaking the hindcast used here, and for making freely available the data sets from this simulation. Data from the RAPID-WATCH MOC monitoring project are funded by the Natural Environment Research Council and are freely available from www.noc.soton.ac.uk/rapidmoc. Data from the Argo project are freely available at www.argo.net, and data from EN3 are freely available at www.metoffice.gov.uk/hadobs/en3. This work was part of the NERC funded RAPID-Watch project MONACO. Lastly, we thank the two anonymous reviewers, whose comments greatly helped to improve the paper.

Edited by: M. Hecht

References

Atkinson, C. P., Bryden, H. L., Hirschi, J. J-M., and Kanzow, T.: On the seasonal cycles and variability of Florida Straits, Ekman and Sverdrup transports at 26° N in the Atlantic Ocean, Ocean Sci., 6, 837–859, doi:10.5194/os-6-837-2010, 2010.

Baringer, M. O. and Molinari, R.: Atlantic Ocean baroclinic heat flux at 24 to 26° N, Geophys. Res. Lett., 26, 353–356, 1999.

Barnett, T. P., Pierce, D. W., AchutaRao, K. M., Gleckler, P. J., Santer, B. D., Gregory, J. M. and Washington, W. M.: Penetration of human-induced warming into the world's oceans, Science, 309, 284–287, 2005.

Bingham, R. J., Hughes, C. W., Roussenov, V., and Williams, G.: Meridional coherence of the North Atlantic meridional overturning circulation, Geophys. Res. Lett., 34, L23606, doi:10.1029/2007GL031731, 2007.

Bjerknes, J.: Atlantic air-sea interactions. Advances in Geophysics, 10, Academic Press, 1–82, 1964.

Bryden, H. L. and Imawaki. S.: Ocean heat transport, in: Ocean Circulation and Climate, edited by: Siedler, G., Church, J., and Gould, J., London, Academic Press, 455–474, 2001.

Bryden, H. L., Longworth, H. R., and Cunningham, S. A.: Slowing of the Atlantic meridional overturning circulation at 25° N, Nature, 438, 655–657 2005.

Cayan, D. R.: Latent and sensible heat flux anomalies over the Northern Oceans: Driving the sea surface temperature, J. Phys. Oceanogr., 22, 859–881, 1992.

Chidichimo, M. P., Kanzow, T., Cunningham, S. A., Johns, W. E., and Marotzke, J.: The contribution of eastern-boundary density variations to the Atlantic meridional overturning circulation at 26.5|degree N, Ocean Sci., 6, 475–490, doi:10.5194/os-6-475-2010, 2010.

Coward, A. C. and de Cuvas, B. A.: The OCCAM 66 level model: Physics, initial conditions and external forcing, SOC internal report, No. 99, 2005.

Cunningham, S. A., Kanzow, T., Rayner, D., Baringer, M. O., Johns, W. E., Marotzke, J., Longworth, H. R., Grant, E. M., Hirschi, J. J.-M., Beal, L. M., Meinen, C. S., and Bryden, H. L.: Temporal Variability of the Atlantic Meridional Overturning Circulation at 26.5° N, Science, 317, 935–938, doi:10.1126/science.1141304, 2007.

Deser, C. and Blackmon, M. L.: Surface climate variations over the North Atlantic Ocean during winter: 1900–1989, J. Climate, 6, 1743–1753, 1983.

Domingues, C. M., Church, J. A., White, N. J., Gleckler, P. J., Wijffels, S. E., Barker, P. M., and Dunn, J. R.: Improved estimates of upper-ocean warming and multi-decadal sea-level rise, Nature, 453, 1090–1093, 2008.

Dong, S. and Kelly K. A.: Heat budget in the Gulf Stream region: The importance of heat storage and advection, J. Phys. Oceanogr., 34, 1214–1231, 2004.

Dong, B. and Sutton, R. T.: Mechanism of Interdecadal Thermohaline Circulation Variability in a Coupled Ocean–Atmosphere OGCM, J. CLimate, 18, 1117–1135, 2005.

Dong, S., Hautala, S. L., and Kelly, K. A.: Interannual variation in upper-ocean heat content and heat transport convergence in the western North Atlantic, J. Phys. Oceanogr., 37, 2682–2697, 2007.

Fasullo, J. T. and Trenberth, K. E.: The Annual Cycle of the Energy Budget, Part II: Meridional Structures and Poleward Transports, J. Climate, 21, 2313–2325 2008.

Feulner, G. and Rahmstorf, S.: On the effect of a new grand minimum of solar activity on the future climate on Earth, Geophys. Res. Lett., 37, L05707, doi:10.1029/2010GL042710, 2010.

Gill, A. E. and Niiler, P. P.: The theory of seasonal variability in the ocean, Deep Sea Res., 20, 141–177, 1973.

Grist, J. P., Marsh, R., and Josey, S. A.: On the relationship between the North Atlantic meridional overturning circulation and the surface-forced overturning stream function, J. Climate, 22, 4989–5002, doi:10.1175/2009JCLI2574.1, 2009.

Grist, J. P., Josey, S. A., Marsh, R., Good, S. A., Coward, A. C., de Cuevas, B. A., Alderson, S. G., New, A. L., and Madec, G.: The roles of surface heat flux and ocean heat transport convergence in determining Atlantic Ocean temperature variability, Ocean Dynam., 60, 771–790. doi:10.1007/s10236-010-0292-4, 2010.

Grossmann, I. and Morgan, M. G.: Tropical cyclones, climate change, and scientific uncertainty: what do we know, what does it mean, and what should be done?, Clim. Change, 108, 543–579, 2011.

Grötzner, A., Latif, M., and Barnett, T. P.: A decadal climate cycle in the North Atlantic Ocean as simulated by the ECHO coupled OGCM, J. Climate, 11, 831–847, 1998.

Hadfield, R. E.: The North Atlantic Study: An Argo based study, Ph.D. thesis, University of Southampton, 198 pp., 2007.

Hadfield, R. E., Wells, N. C., Josey, S. A., and Hirschi J. J.-M.: On the accuracy of North Atlantic temperature and heat storage fields from Argo, J. Geophys. Res., 112, C01009, doi:10.1029/2006LC003825, 2007.

Hirschi, J. J.-M., Baehr, J. Marotzke, J., Stark, J., Cunningham, S., and Beismann, J.-O.: A monitoring design for the Atlantic meridional overturning circulation, Geophys. Res. Lett., 30, 1413, doi:10.1029/2002GL016776, 2003.

Hirschi, J. J.-M., Killworth, P. D., and Blundell, J. R.: Subannual, Seasonal, and Interannual Variability of the North Atlantic Meridional Overturning Circulation, J. Phys. Oceanogr., 37, 1246–1265, 2007.

Hirschi, J. J.-M., Killworth, P. D., and Blundell, J. R.:: Sea surface height signals as indicators for oceanic meridional mass transports, J. Phys. Oceanogr., 39, 581–601, 2009.

Hoyos, C. D, Agudelo, P. A., Webster, P. J., and Curry, J. A.: Deconvolution of the Factors Contributing to the Increase in Global Hurricane Intensity, Science, 312, 94–97, 2006.

Huerta-Casas A. M. and Webb, D. J.: High frequency fluctuations in the heat content of an ocean general circulation model, Oc. Sci., 8, 813–825, doi:10.5194/os-8-813-2012, 2012.

Ingleby, B., and M. Huddleston, 2007. Quality control of ocean temperature and salinity profiles - historical and real-time data. Journal of Marine Systems, 65, 158-175 10.1016/j.jmarsys.2005.11.019

Jayne, S. R. and Marotzke, J.: The Dynamics of Ocean Heat Transport Variability, Rev. Geophy., 39, 385–411, 2001.

Johns, W., Bryden, H., Baringer, M., Beal, L., Cunningham, S., Kanzow, T., Hirschi, J., Marotzke, J., Garraffo, Z., Meinen, C., and Curry, R.: Continuous, array-based estimates of Atlantic Ocean heat transport at 26.5° N, J. Climate, 24, 2429–2449. doi:http://dx.doi.org/10.1175/2010JCLI3997.1, 2011.

Josey, S. A.: A comparison of ECWMF, NCEP-NCAR and SOC surface fluxes with moored buoy measurements in the subduction region of the Northeast Atlantic, J. Climate, 14, 1780–1789, 2001.

Josey, S. A., Grist, J. P., and Marsh, R.: Estimates of meridional overturning circulation variability in the North Atlantic from surface density flux fields, J. Geophys. Res., 114, C09022, doi:10.1029/2008JC005230, 2009.

Kanzow, T., Cunningham, S., Rayner, D., Hirschi, J., Johns, W.E., Baringer, M., Bryden, H., Beal, L., Meinen, C., and Marotzke, J.: Flow compensation associated with the meridional overturning circulation, Science, 317, 938–941, doi:10.1126/science.1141293, 2007.

Kanzow T., Johnson, H., Marshall, D., Cunningham, S. A., Hirschi, J. J.-M., Mujahid, A., Bryden, H. L., and Johns, W. E.: Basin-wide integrated volume transports in an eddy-filled ocean, J. Phys. Oceanogr., 39, 3091–3110, 2009.

Kanzow, T., Cunningham, S., Johns, W. E., Hirschi, J. J.-M., Marotzke, J., Baringer, M., Meinen, C., Chidichimo, M. P., Atkinson, C., Bryden, H., and Collons, J.: Seasonal variability of the Atlantic meridional overturning circulation at 26.5° N, J. Climate, 23, 5678–5698, doi:10.1175/2010JCLI3389.1, 2010.

Klotzbach, P. J.: Recent developments in statistical prediction of seasonal Atlantic basin tropical cyclone activity, Tellus, 59A, 511–518, 2007.

Kump, L. R., Kasting, J. F., and Crane, R. G.: The Earth System, Upper Saddle River NJ, Prentice Hall, 1999.

Kushnir, Y.: Interdecadal variations in the North Atlantic sea surface temperature and associated atmospheric conditions, J. Climate, 7, 141–157, 1994.

Large, W. G., Danabasoglu, G., and Doney, S. C.: Sensitivity to surface forcing and boundary layer layer mixing in a global ocean model: annual-mean climatology, J. Phys. Oceanogr., 27, 2418–2446, 1997.

Lozier, M. S., Leadbetter, S., Williams, R. G., Roussenov, V., Reed, M. S. C., and Moore, N. J.: The Spatial Pattern and Mechanisms of Heat-Content Change in the North Atlantic, Science, 319, 800–803, 2008.

Lyman, J. M., Good, S. A., Gouretski, V. V., Ishii, M., Johnson, G. C., Palmer, M. D, Smith, D. M., and Willis, J. K.: Robust warming of the global upper ocean, Nature, 465, 334–337, 2010.

Mainelli, M., Demaria, M., Shay, L. K., and Goni, G.: Application of Oceanic Heat Content Estimation to Operational Forecasting of Recent Atlantic Category 5 Hurricanes, Weather and Forecasting, 23, 3–16, 2008.

Marotzke, J., Cunningham, S. A., and Bryden, H. L.: Monitoring the Atlantic meridional overturning circulation at 26.5° N, available at: http://www.noc.soton.ac.uk., 2002.

Marsh, R., Josey, S. A., de Cuevas, B. A., Redbourn, L. J., and Quartly, G. D.: Mechanisms for recent warming of the North Atlantic: Insights gained with an eddy-permitting model, J. Geophys. Res., 114, C04031, doi:10.1029/2007JC004096, 2008.

Marsh, R., de Cuevas, B. A., Coward, A. C., Jacquin, J., Hirschi, J. J.-M., Aksenov, Y., Nurser, A. J. G., and Josey, S. A.: Recent changes in the North Atlantic circulation simulated with eddy-permitting and eddy-resolving ocean models, Oc. Modell., 28, 226–239, 2009.

McCarthy, G. D., Frajka-Williams, E., Johns, W. E., Baringer, M. O., Meinen, C. S., Bryden, H. L., Rayner, D., Duchez, A., Roberts, C. D., and Cunningham, S. A.: Observed interannual variability of the Atlantic meridional overturning circulation at 26.5° N, Geophys. Res. Lett., 39, L19609, doi:10.1029/2012GL052933, 2012.

Rayner, D., Hirschi, J. J.-M., Kanzow, T., Johns, W. E., Wright, P. G., Frajka-Williams, E., Bryden, H. L., Meinen, C. S., Baringer, M. O., Marotzke, J., Beal, L. M., and Cunningham, S. A.: Monitoring the Atlantic Meridional Overturning Circulation, Deep-Sea Res. Pt. II, 58, 1744–1753. doi:10.1016/j.dsr2.2010.10.056, 2011.

Scaife, A. A. and Knight, J. R.: Ensemble simulations of the cold European winter of 2005–2006, Q. J. R. Meteorol., 134, 1647–1659, 2008.

Seager, R., Kushnir, Y., Visbeck, M., Naik, N., Miller, J., Krahmann, G., and Cullen, H.: Causes of Atlantic Ocean Climate Variability between 1958 and 1988, J. Climate, 13, 2845–2862, 2000.

Tompkins A. M. and Feudale, L.: Seasonal ensemble predictions of West African monsoon precipitation in the ECMWF System 3 with a focus on the AMMA special observing period in 2006, Weather and Forecasting, 25, 768–788, doi:10.1175/2009WAF2222236.1, 2010.

Trenberth, K. E. and Caron, J. M.: Estimates of meridional atmosphere and ocean heat transports, J. Climate, 14, 3433–3443, 2001.

Vivier, F., Kelly, K. A., and Thompson, L.: Heat budget in the Kuroshio extension region: 1993–1999, J. Phys. Oceanogr., 22, 3436–3454, 2002.

Warren, B. A.: Approximating the energy transport across oceanic sections, J. Geophys. Res., 104, 7915–7920, 1999.

Wells, N. C., Josey, S. A., and Hadfield, R. E.: Towards closure of regional heat budgets in the North Atlantic using Argo floats and surface flux datasets, Ocean Sci., 5, 59–72, doi:10.5194/os-5-59-2009, 2009.